Received: 23 June 2023 | Revised: 6 July 2023 | Accepted: 22 August 2023

DOI: 10.1002/pamm.202300037

RESEARCH ARTICLE

On the load bearing mechanisms of cemented granular material: A mesoscale FE approach

Michail Komodromos[1] | **Mahan Gorji**[2] | **Alexander Düster**[2] | **Jürgen Grabe**[1]

[1]Institute of Geotechnical Engineering and Construction Management (B-5), Hamburg University of Technology, Hamburg, Germany

[2]Numerical Structural Analysis with Application in Ship Technology (M-10), Hamburg University of Technology, Hamburg, Germany

Correspondence
Michail Komodromos, Institute of Geotechnical Engineering and Construction Management (B-5), Hamburg University of Technology, Harburger Schloßstraße 36, 21079 Hamburg, Germany.
Email: michail.komodromos@tuhh.de

Funding information
DFG, Grant/Award Numbers: GR 1024/41-1, DU 405/17-1

Abstract

The numerical investigation of cemented granular material (CGM) is a demanding task that requires the combination of various scientific disciplines. At the mesoscale, CGM is decomposed into the constituents of particles, cement matrix and void pores. The combination of these constituents, as found in nature or in civil infrastructure projects, creates a highly heterogeneous structure, whose morphology defines the response of the CGM under mechanical loading. The composite internal structure is quantified by means of x-ray Computed Tomography, which provides 16-bit grayscale 3D images of the scanned microsamples. These images are decomposed into the three constituent materials to be investigated and modeled. Still, the ability of simple Cartesian grids to adequately carry information about curved geometries and provide accurate representations is questioned. In order to overcome staircase effect errors, the interfaces of the material inclusions are smoothed and re-defined, making use of Gaussian blurred signed distance fields (SDF). These level-set derived interfaces serve as a reference for the volume reconstruction of the image via tetrahedra. The comparison of the raw and the smoothened images to analytical geometry Standards suggests that the above reconstruction alleviates the grid's inherited uncertainities. In addition, a comparison between a non smoothed and a smoothed meshed image is performed in terms of mechanical response, utilizing the Finite Element (FE) Method. The results suggest that even a slight change in the granular contact fabric can alter the unfolding stress transmission mechanisms.

1 | INTRODUCTION

The morphological and mechanical investigation of composites is a challenging field for scientists and engineers. During the last decades, the structure of such materials is quantified via approaches that combine non destructive scanning modalities with three-dimensional image reconstruction algorithms, such as x-ray Computed Tomography [1]. In the specific case of granular materials, the image processing and evaluation are not trivial, because of the randomness that characterizes the shape and position of the incorporated particles. Due to the design of emission detectors, the reconstruction of the images is done using a Cartesian grid (Figure 1A), which leads to geometrical inaccuracies, with impact on the actual measurements made. One step beyond, such grid bias can be transmitted to an equivalent image based simulation.

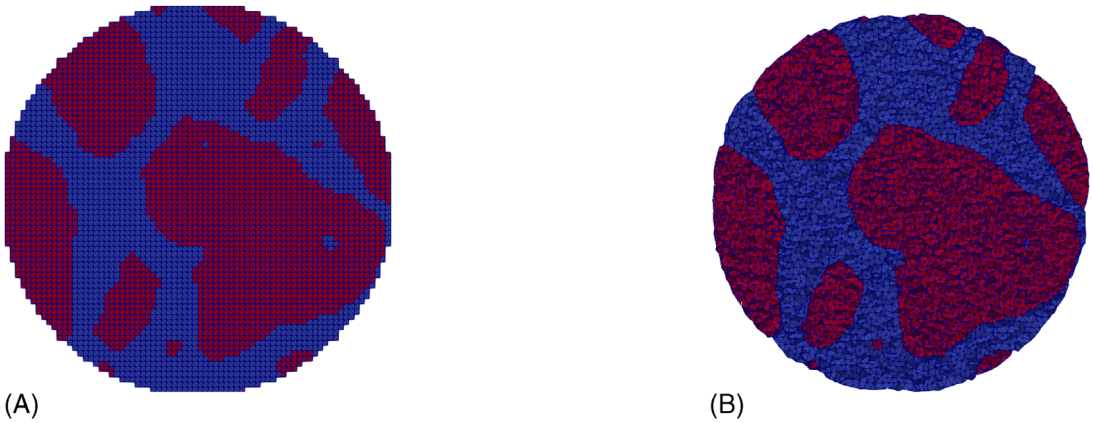

FIGURE 1 Image subdomain of cemented sand material: (A) voxel model, (B) tetrahedral mesh.

In this attempt, the transition from the typical Cartesian grid of the images to a tetrahedral mesh, as shown in Figure 1B is presented and applied to a cylindrical subdomain of cemented sand material. The segmented image is transformed into a continuous field that carries the phase interface information. Light blurring is applied to this continuous field to achieve the smoothening and the new, debiased interfaces are extracted. This information serves as a reference for volume reconstruction using tetrahedra and the final image outcome is verified by comparison to analytical geometry standards. Ultimately, it is suggested that such transition grants greater objectivity to image measurements and aids image based numerical modeling.

2 | FROM VOXEL IMAGES TO EQUIVALENT SMOOTH CONTINUOUS FIELDS

The internal geometry of the scanned composite is related to the material phase boundaries. As displayed in Figures 1 (A,B), the current material configuration consists of three distinct interfaces between particles and matrix, particles and surrounding void, cement and surrounding void. Despite the fact that such boundary is easily distinguishable and can be derived via basic image analysis processes (signed distance field [SDF] [2, 3], gradient [4]), the grid representation of the images carries biases. Specifically, uncertainty accumulates at positions of curved interfaces. Moreover, the cylindrical boundaries of the domain are roughly captured. The staircase effect at the external boundaries provides visual evidence of the weakness of a Cartesian grid to quantify curvature. Solutions for this problem are proposed for analytically defined objects, like spheres [5], by introducing non-binary imaged shapes, whose edge surfaces partition the encountered voxels. Nevertheless, in cases of arbitrary shaped objects, like sand particles, the imaged structures can be better handled by altering the representation framework itself.

The piece-wise continuous three-dimensional segmented images are reconstructed by alternative geometrical entities; tetrahedra, from now referred to as *tet4*. The choice of these geometrical entities is justified by their capacity to efficiently discretize any arbitrary geometry in three dimensions [6], which is not the case for cuboidal voxels. The bias of the Cartesian grid can be visually conceived as the staircase effect, which is evident even in high resolutions. In order to derive the exact morphology of the scanned multiphased object, the signed distance field, from now on referred to as *SDF* (Equation (1)), is individually applied to each label k and its corresponding volume Ω_k of the solid phases (Figures 2A,C).

$$\forall k, \quad SDF_k(\boldsymbol{x}) = \begin{cases} d(\boldsymbol{x}, \partial\Omega_k), & \text{if } \boldsymbol{x} \in \Omega_k \\ -d(\boldsymbol{x}, \partial\Omega_k), & \text{if } \boldsymbol{x} \notin \Omega_k \end{cases} \tag{1}$$

where d represents the Euclidean distance.

In spite of being continuous, these fields inherit the staircase effect, as can be observed at the interfaces of the inclusions. In order to smoothen these boundaries, a light Gaussian blur filter was applied (Figures 2B, D), which effectively tackles the staircase effect and captures the information of edges angularity [7]. The extraction of the 3D envelope surfaces took

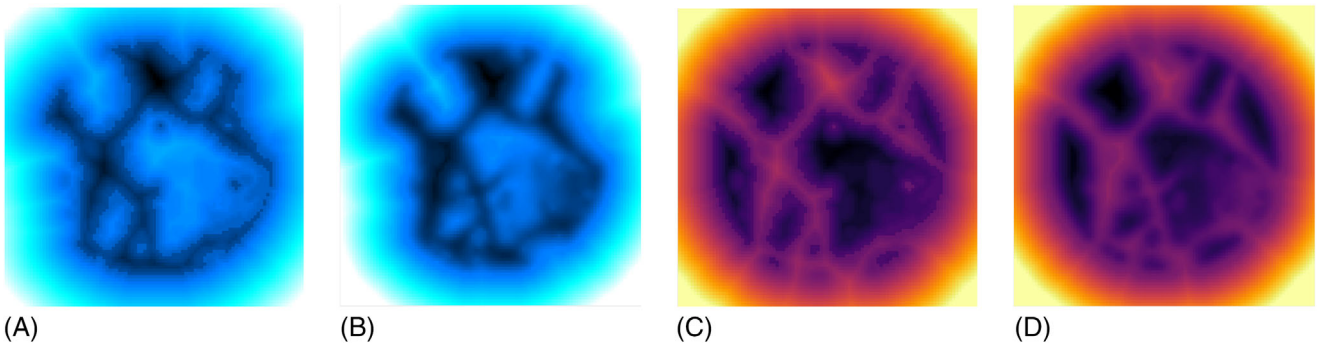

FIGURE 2 Distance fields: (A) cement matrix (sharp), (B) cement matrix (smooth), (C) particles (sharp), (D) particles (smooth).

FIGURE 3 Three-dimensional object representations: (A) voxel image, (B) sharp *tet4* image, (C) smooth *tet4* image.

place by deriving the level-set function at the value of 0, as defined in Equation (2). Such magnitude corresponds exactly to the boundary of the segmented material chosen, according to the definition of the SDF given before. The above process was realized by using the SDF generation, as implemented in the open source code software for practical analysis of materials (SPAM) [8] and the Marching Cubes algorithm [9], adjusted to the value of zero, as implemented in the open source library SciPy [10]. The output object is a very fine triangulated surface, which can be efficiently manipulated via the information of its nodal positions and connectivity.

$$\forall k, \quad LS(SDF_k) = \{\boldsymbol{x} \quad | \quad SDF_k(\boldsymbol{x}) = 0\}, \quad \boldsymbol{x} \quad \in \quad \Omega \tag{2}$$

3 | TRANSITION TO TETRAHEDRAL MESHES

After the smooth re-definition of the material inclusions, the envelope surfaces allow for the volume reconstruction of the enclosed bulk. At a first step, a *tet4* approximation of the volume is realized by using the open source library computational geometry algorithm library (CGAL) [11], which produces an approximation of the solid material distinguished image (Figure 3A) in the form of a *tet4* mesh (Figure 3B). This approximation is based on the sharp inclusion interfaces [12] and is modified by an element optimization scheme [13], which improves the shape of the *tet4*, sometimes at the expense of the precise morphological equivalence. In order to avoid this, the interface nodes of each material phase are projected onto the corresponding smoothened material envelope surface, adjusting the mesh to fit exactly the interfaces derived from the blurred distance fields. Ultimately, the process produces a smooth *tet4* image (Figure 3C).

Apart from the alleviation of staircased material boundaries, the transition from a Cartesian grid to a *tet4* adaptive mesh offers objectivity in volume representation. Vertical slices extending from the center of the image to the cylinder edges were

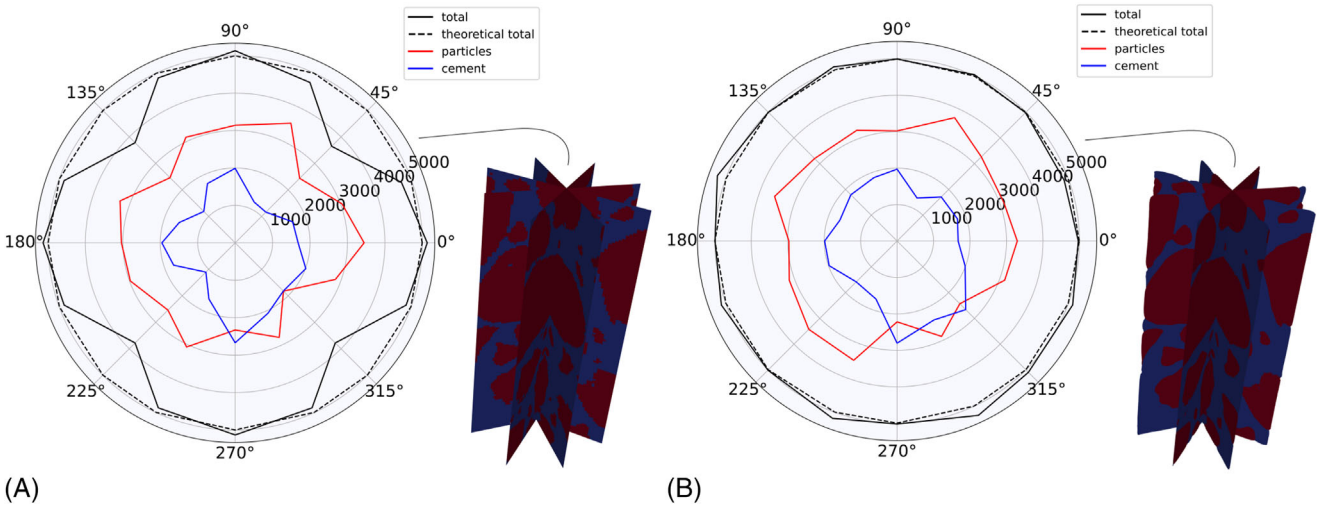

FIGURE 4 Vertical slices area: (A) voxel image, (B) tetrahedral image.

studied at different angles. For each of these slices, the total area and the area of the constituent phases were computed via basic pixel counting (Figure 4A). It is shown that for the grid aligned directions of 0, 90, 180 and 270 degrees, the surface area of the slices agrees well with the theoretical surface area. On the other hand, the surface of the slice decreases in any other direction, reaching local minima at the inclinations of 45, 135, 225 and 315 degrees. In contrast, the equivalent *tet4* image shows quite better output by being closer to the theoretical slice surface at any direction (Figure 4B). It is worth noticing that the bias affects the phase presence in a non analogous manner. It can be concluded that the amounts of particle volume and cement mortar are not correlatable between the two volume representations on the 45, 135, 225 an 315 degrees oriented slices.

4 | MECHANICAL SIMULATION OF IMAGE DERIVED TOPOLOGIES

The transition from voxel grids to *tet4* meshes offers another convenient feature; the scanned object is represented in a manner suitable for a Finite Element (FE) solver. In addition, the solving process becomes quite efficient, thanks to *tet4* elements. Numerical tests are performed in a FE framework using the commercial code Abaqus Standard [14], by assigning the corresponding boundary conditions. Uniaxial compression tests are conducted, in order to evaluate the capacity of linear elastic mesoscale simulation to capture unfolding mechanisms. Furthermore, a comparison between sharp and smooth edged tetrahedral equivalents is made to estimate the influence of smoothening the simulation output. In both domain versions, the numbers of nodes and elements are kept exactly the same. The visual inspection of the sharp and smooth versions suggests a close match. The shape and size of the material inclusions seem to remain the same. On the other hand, it can be noticed that the surface roughness is altered. The contact fabric is also slightly different in the two versions; the smooth representation presents more contact points and greater touching surface areas (Figure 5).

In both cases, the load bearing mechanisms are in accordance with published numerical evidence in granular micromechanics, which suggests the formation of intergranular transmission chains [15], but presents quantitative differences between the sharp and the smooth versions. Intergranular load transmission is evident, which presents high stress localization at the contact points. Considering shape and size, larger particles seem to attract greater magnitudes of stress. Despite the size, a condition to contribute to the load arrangement relies on having contacts that are oriented to the external loading direction. Furthermore, the cement matrix aids the load transfer by forming stress bridges in the region in between close positioned grains. In a similar fashion, the distant contact area needs to be closely aligned to the loading direction to be mobilized, this time with the help of the cement medium. Proceeding into the actual load distribution through the bulk of the particle, bulbs are displayed, which have a quite close resemblance to the results of experiments utilizing photoelasticity. Comparing the two versions, qualitatively and quantitatively, the following conclusions can be drawn. First, staircase inherited roughness on the interfaces does not seem to alter the stress states

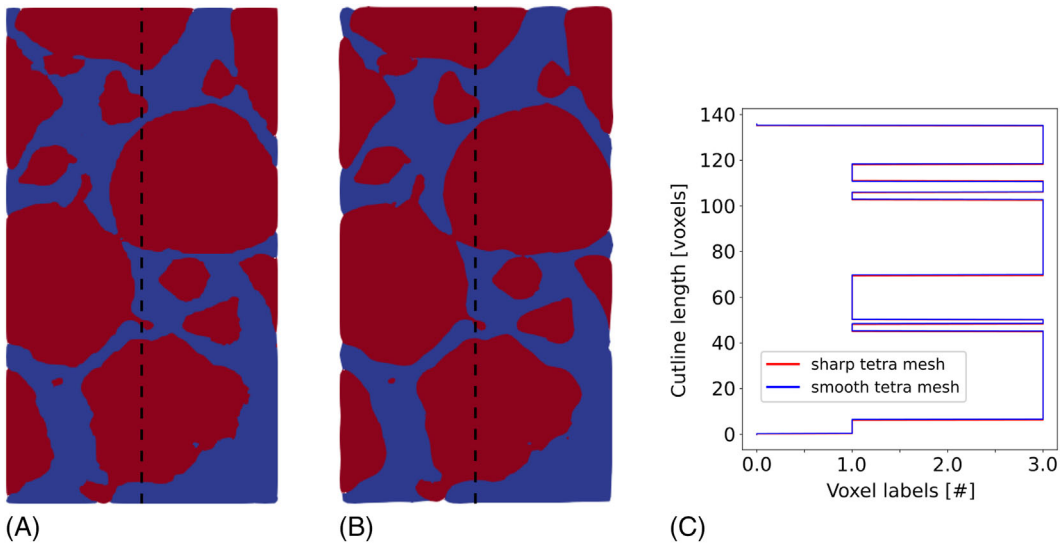

FIGURE 5 Tetrahedral image domains: (A) sharp edged mesh, (B) smooth edged mesh, (C) phase cutline.

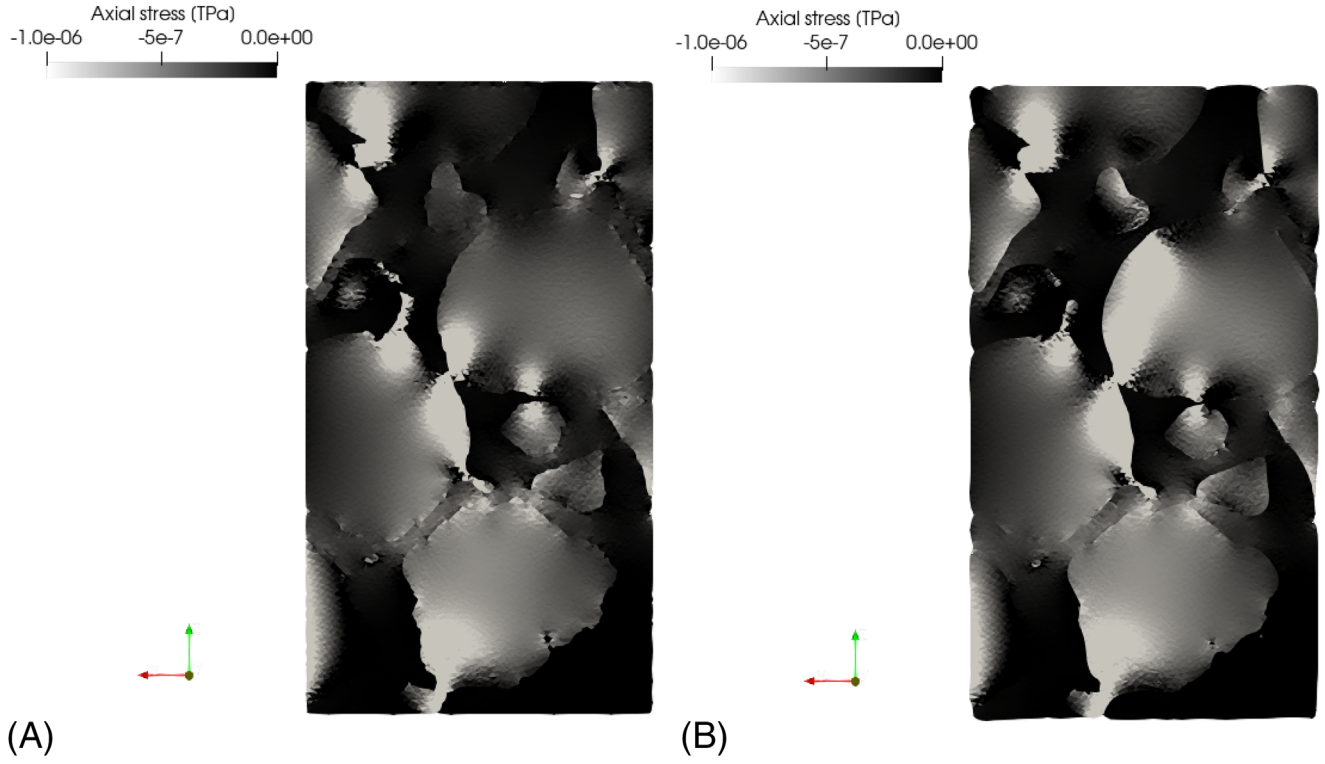

FIGURE 6 Intergranular stress transmission: (A) sharp edged mesh, (B) smooth edged mesh.

in the close neighborhood of these regions. Apart from the smooth particle shape, the smoothening does not seem to change the magnitudes or the distribution of stresses close to the borders of the materials. It should be highlighted that this conclusion refers to this specific case of externally loading an assembly of particles. Second, the smooth version presents a slightly diverse prediction of the stress chain formation. This can be justified by the slightly diverse granular contact network it presents. It is quite probable that the truth lies in between the two predictions. Still, what is important to be highlighted by the evidence above is the significance of the contact network [16]. Even the lightest modification of it can lead to quite a different stress distribution and thus to a different response (Figure 6).

5 | CONCLUSIONS

This work addresses the metrological and the numerical perspectives offered by the transition from voxel to tetrahedral three-dimensional images. The grid framework of segmented images fails to display accurate information about curved boundaries, due to the inability of cuboids to efficiently approximate arbitrarily shaped objects. Such representation can cause the following issue; at non Cartesian aligned directions, there seems shape distortion to happen, which does not allow the local volume measurements and investigations.

The segmented image was decomposed into the constituent materials of the cement matrix and the particle assembly. Each component was transformed into a continuous SDF that carries the information of each solid material boundary. The surrounding air is explicitly skipped in this procedure. A Gaussian blur filter on these fields rectified the staircase effect on the boundaries, which were extracted from scratch by the Marching Cubes algorithm. Based on this smoothed redefinition of edges, the solid volume was reconstructed by tetrahedra, which linearly approximate the enclosed volumes. A simple comparison of the total volume of the two representations with analytical geometry standards suggests that the *tet4* images display information which is quite close to the actual topology. As a result, they present objectivity in any radial direction chosen to locally analyze the cylinder.

Finally, mechanical simulations of uniaxial compression tests were performed to draw conclusions on the influence of the smoothed interfaces on the mesoscale unfolding mechanisms. The stress output suggests that smoothening does alter the stress distribution, but not on the material interfaces. Its application causes a slight change in the granular fabric, which results in a relocation and reform of the stress transmitting chains. Such evidence shows how sensitive mesoscale mechanical simulation of CGM can be, but at the same time it supports the statement that fabric is the dominant morphological property which defines the response of coarse geomaterials. Future work shall focus on the derivation of mass associated equivalents, such as the center of mass, the sphericity and the inertia tensors of incorporated particles based on tetrahedral images and its comparison with measurements made directly on segmented voxel volumes.

ACKNOWLEDGMENTS

The authors gratefully acknowledge the financial support provided by the DFG (Deutsche Forschungsgemeinschaft) under the grant numbers GR 1024/41-1 and DU 405/17-1 and the beam time provided by Laboratoire 3SR, Grenoble, France and are grateful to Olga Stamati and Pascal Charrier for their help in the X-ray scanning procedure.

Open access funding enabled and organized by Projekt DEAL.

ORCID

Michail Komodromos https://orcid.org/0000-0003-4408-216X
Mahan Gorji https://orcid.org/0000-0002-0722-1573

REFERENCES

1. Desrues, J., Viggiani, G., & Besuelle, P. *Advances in X-ray tomography for geomaterials* Wiley, New York.
2. Chan, T., & Zhu, W. (2005). Level set based shape prior segmentation. In *2005 IEEE computer society conference on computer vision and pattern recognition CVPR* (Vol. *2*, pp. 1164–1170). IEEE.
3. Malladi, R., Sethian, J. A., & Vemuri, B. C. (1995). Shape modeling with front propagation: a level set approach. *IEEE Transactions on Pattern Analysis and Machine Intelligence*, *17*, 158–175.
4. Canny, J. (1986). A computational approach to edge detection. *IEEE Transactions on Pattern Analysis and Machine Intelligence*, *8*, 679–698.
5. Tengattini, A., & Andó, E. (2015). Kalisphera: an analytical tool to reproduce the partial volume effect of spheres imaged in 3D. *Measurement Science and Technology*, *26*, 095606.
6. Bukenberger, D. R., & Lensch, H. P. A. (2021). Tetrahedra of varying density and their applications. *The Visual Computer*, *37*, 2447–2460.
7. Rorato, R., Arroyo, M., Andó, E., & Gens, A. (2019). Sphericity measures of sand grains. *Engineering Geology*, *254*, 43–53.
8. Stamati, O., Andó, E., & Roubin, E. (2020). SPAM: software for practical analysis of materials. *Journal of Open Source Software*, *5*, 2286.
9. Lorensen, W. E., & Cline, H. E. (2019). Marching cubes: a high resolution 3D surface construction algorithm. *ACM SIGGRAPH Computer Graphics*, *21*, 163–169.
10. Virtanen, P., Gommers, R., & Oliphant, T. E. (2020). SciPy 1.0: fundamental algorithms for scientific computing in Python. *Nature Methods*, *17*, 261–272.
11. Alliez, P., Jamin, C., Rineau, L., Tayeb, S., Tournois, J., & Yvinec, M. (2023). 3D Mesh Generation. CGAL User and Reference Manual.
12. Boissonnat, J. D., & Oudot, S. Y. (2005). Provably good sampling and meshing of surfaces. *Graph Models*, *67*, 405–451.
13. Pons, J. P., Ségonne, E., Boissonnat, J. D., Rineau, L., Yvinec, M., & Keriven, R. (2007). High-quality consistent meshing of multi-label datasets. *Information Processing in Medical Imaging*, *20*, 198–210.

14. Smith, M. *ABAQUS/Standard User's Manual* (Dassault Systémes Simulia Corp).
15. Cundal, P. A., & Strack, O. D. L. (1979). A discrete numerical model for granular assemblies. *Géotechnique*, *29*, 47–65.
16. Wiebicke, M., Andó, E., Herle, I., & Viggiani, G. (2017). On the metrology of interparticle contacts in sand from X-ray tomography images. *Measurement Science and Technology*, *28*, 124007.

How to cite this article: Komodromos, M., Gorji, M., Düster, A., & Grabe, J. (2023). On the load bearing mechanisms of cemented granular material: A mesoscale FE approach. *Proceedings in Applied Mathematics and Mechanics*, *23,* e202300037. https://doi.org/10.1002/pamm.202300037